







G-Quadruplex-Forming Aptamers as Selective Inhibitors of HMGB1 Protein: a Journey from Design to Their Functional Validation

 Ettore Napolitano,  Andrea Criscuolo,  Claudia Riccardi,  Chiara Platella,
 Domenica Musumeci,*  Daniela Montesarchio#

Department of Chemical Sciences, University of Naples Federico II, via Cintia 21, 80126 Napoli, Italy

* Corresponding author's e-mail address: domenica.musumeci@unina.it

Corresponding author's e-mail address: daniela.montesarchio@unina.it

RECEIVED: June 19, 2025 * REVISED: October 14, 2025 * ACCEPTED: October 26, 2025

PROCEEDING OF THE SOLUTIONS IN CHEMISTRY 2024, 11–15 NOVEMBER 2024, SVETI MARTIN NA MURI, CROATIA

Abstract: High Mobility Group Box 1 (HMGB1) is a multifunctional nuclear protein which, extracellularly released, acts as a pro-inflammatory alarmin implicated in inflammatory, autoimmune and cancer-related pathologies. This review provides a detailed account on G-quadruplex (G4)-forming aptamers targeting HMGB1 and inhibiting HMGB1-induced cell migration. A SELEX-based approach allowed identifying a set of G4-forming anti-HMGB1 aptamers, with L12 as the most promising one forming monomeric hybrid along with dimeric parallel G4 structures. The latter forms displayed higher affinity and activity towards HMGB1 but, upon annealing, were irreversibly converted into less active monomeric G4 structures. Covalently linked L12 dimers were designed to lock the most bioactive species, with L12d1T3 as the best candidate forming unimolecular parallel G4 structures featured by reversible folding/unfolding, marked affinity for HMGB1 and high serum resistance. These findings highlight the role of G4 structuring in anti-HMGB1 activity, showcasing covalently linked dimeric aptamers as tools for HMGB1-targeted therapy and diagnostics.

Keywords: aptamers, G-quadruplex structures, HMGB1, dimerization.

INTRODUCTION

HIGH MOBILITY GROUP BOX 1 (HMGB1) is a highly conserved, non-histone nuclear small protein abundantly present in eukaryotic nuclei.^[1,2] Human HMGB1 consists of 215 amino acids with two tandem domains, known as HMG boxes A and B, and an acidic C-terminal tail.^[3,4] The A and B boxes of the protein can interact with DNA, thus producing either bending or distortion of the double helix,^[3–5] whereas the acidic C-terminus contributes to the spatial arrangement of both A and B boxes and regulates HMGB1-DNA binding specificity^[6] (Figure 1). Under physiological conditions, HMGB1 plays a fundamental role in chromatin remodelling, gene transcription regulation, and DNA repair.^[7–12] Notably, when released into the extracellular environment - either passively by necrotic cells or actively by immune cells in response to inflammatory stimuli -

HMGB1 acts as an alarmin.^[13–15] In this context, it binds pattern recognition receptors such as the Receptor for Advanced Glycation End-products (RAGE)^[16–18] and Toll-like receptors (TLR2, TLR4),^[19,20] thereby promoting inflammation and immune cell recruitment. HMGB1 is implicated in the pathogenesis of a wide range of inflammatory, autoimmune, and neoplastic diseases.^[21] High extracellular HMGB1 levels have been observed in sepsis,^[22,23] rheumatoid arthritis,^[24] Alzheimer's disease,^[10–12] and various types of cancer, including melanoma,^[25] colorectal,^[26] pancreatic,^[27] lung^[28] and breast cancer.^[29] Moreover, its central role in triggering cytokine storms and acute respiratory distress syndrome (ARDS) has also made it a potential target in severe COVID-19 cases.^[30]

Despite its well-documented clinical relevance, the development of effective and selective HMGB1 inhibitors remains a challenge.^[31,32] In fact, the known HMGB1

inhibitors reported in the literature have some limitations. Among small molecules, glycyrrhizin is characterized by poor oral bioavailability^[33] and adverse effect on chronic use, like fluid retention and hypertension.^[34] Diflunisal, another non-steroidal anti-inflammatory drug, carries risks of gastrointestinal toxicity, renal impairment, and cardiovascular events.^[35] Peptide inhibitors, such as HBP08, are generally characterized by low plasma stability and low bioavailability.^[36] Finally, monoclonal antibodies typically display chemical/enzymatic instability, batch-to-batch variability and potential immunogenicity. These drawbacks strongly highlight the need for novel HMGB1-targeting agents based on more stable and selective molecules endowed with improved pharmacological profiles and capable of modulating pathological HMGB1 activities without interfering with its physiological functions.

In this scenario, DNA-based aptamers - i.e. short synthetic single-stranded oligonucleotides featured by high affinity and specificity for a given target – represent a valuable, promising strategy.^[37] In particular, aptamers have gained interest due to their generally high chemical stability, low immunogenicity and batch-to-batch variability, as well as ability to form well-defined tertiary structures.^[38–42] These features make them ideal candidates for selectively targeting proteins,^[43] especially circulating ones such as HMGB1 in pathological conditions, since in this case aptamers are not required to cross cell membranes to exert their bioactivity.

Considering the ability of HMGB1 to recognize with high affinity a wide range of distorted DNA structures - such as cis-platinated, UV-damaged or cruciform DNA^[44] - the first DNA-based anti-HMGB1 ligands were obtained by rationally designing properly kinked DNA duplex structures.^[45,46] The insertion of unpaired adenines in the middle of one of the two strands was exploited to produce asymmetric internal bulges, which allowed the desired bending in the duplex structure. Interestingly, these ligands showed ability to bind HMGB1 with high affinity and inhibit HMGB1-induced cell proliferation and migration in a concentration-dependent manner.^[46] However, the thermal stability of their tertiary structure was quite low. Thus, considering that unimolecular structures are generally more thermally and enzymatically resistant than bimolecular ones,^[47,48] a bent hairpin-loop DNA was designed as an optimized, unimolecular version of the previously studied kinked bimolecular duplex.^[49] This hairpin-loop duplex showed good thermal and enzymatic stability, still efficiently interacting with HMGB1 protein. Moreover, it was also able to inhibit the protein-induced cellular migration in a concentration-dependent manner and with very high efficiency.^[49]

Subsequently, in a pull-down experiment from a human cellular nuclear extract, HMGB1 has been proved to recognize not only bent duplexes but also G-quadruplex

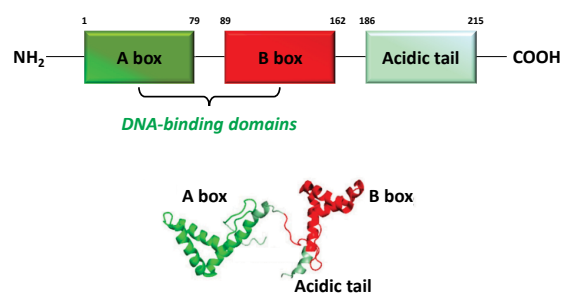


Figure 1. Representation of the HMGB1 structure with indication of the functionally relevant regions of the protein.

(G4)-forming oligonucleotides, such as the 26-mer truncation of the human telomeric sequence (tel₂₆)^[50,51] and a G-rich oligonucleotide taken from the promoter region of the *KRAS* oncogene.^[52] These discoveries have been particularly relevant for our recent research and stimulated us to develop novel effective HMGB1 ligands based on these peculiar nucleic acid secondary structures.

Selection and Characterization of Anti-HMGB1 Aptamers Forming G-Quadruplex Structures

Taking inspiration from the previous findings on the ability of HMGB1 to recognize in cell systems also G4 structures,^[50–52] we employed a SELEX-like procedure specifically tailored to direct the selection of anti-HMGB1 aptamers towards G4-forming oligonucleotides (Figure 2).^[53] The initial DNA library was based on a guanine-rich core derived from the telomeric sequence 5'-TTA(GGGTTA)₃GGGT-3', (tel₂₆), previously proved to interact with HMGB1.^[50,51] Specifically, the library core included four GGG tracts, alternated with regions of three variable bases (with restriction to thymines and adenines) repeated three times. The TTA and TT bases at the 5'- and 3'-ends, respectively, were maintained in analogy to tel₂₆ so to finally obtain the general sequence 5'-TTA(GGGXXX)₃GGGT-3', with X = A or T. Suitable complementary primer sequences were inserted at both the 5'- and 3'-ends to allow the amplification of the selected oligonucleotides by PCR. Nickel-Nitriloacetic acid (Ni-NTA) magnetic agarose beads were used for the partitioning step of the SELEX cycle, allowing the easy magnetic separation of the HMGB1-bound sequences from the unbound ones. Before the incubation with the His-tagged protein, the library sequences were first heated at 85 °C for 5 min, then immediately cooled on ice for 2 min to favour the formation of intramolecular oligonucleotide structures. By performing first a negative selection against the Vascular Endothelial Growth Factor (VEGF-A), a protein present at high concentration in the serum of patients with various cancer types,^[54] and then a positive target

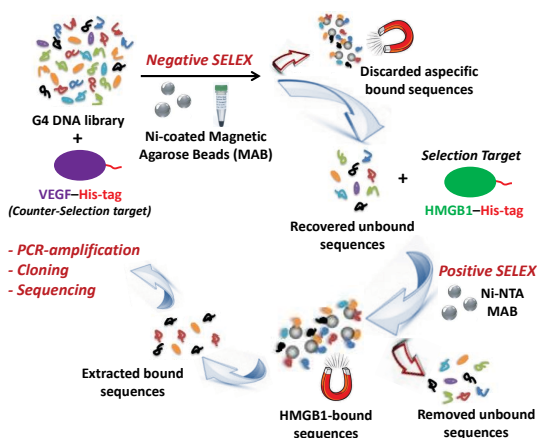


Figure 2. Schematic representation of the SELEX procedure we adopted for the selection of anti-HMGB1 aptamers. The figure is from Napolitano et al.,^[53] with permission.

enrichment using HMGB1 (Figure 2), 14 oligonucleotides were finally isolated, whose sequences are listed in Table 1.

Notably, in the explored conditions, tel₂₆ was not present among the 14 selected sequences, probably because it was discarded during the counter-selection process with VEGF₁₆₅ or because of its lower affinity for HMGB1 compared to the other 14 selected sequences.

The successive physico-chemical investigation in a pseudo-physiological solution (PBS, phosphate buffer saline) mimicking the extracellular milieu, demonstrated

Table 1. Oligonucleotide sequences identified by SELEX as anti-HMGB1 aptamers.

Name	Sequence
A32	5'-TTAGGGTTAGGGAATGGGATAGGGTT-3'
B6	5'-TTAGGGATAGGGTTTGGGATAGGGTT-3'
D40	5'-TTAGGGTATGGGTATGGGATTGGGTT-3'
L12	5'-TTAGGGATTGGGAATGGGTATGGGTT-3'
L13	5'-TTAGGGTATGGGAAAGGGTAAGGGTT-3'
L16	5'-TTAGGGAAGGGTTAGGGAAGGGTT-3'
L17	5'-TTAGGGTATGGGATAGGGTATGGGTT-3'
L21	5'-TTAGGGTTAGGGTAAGGGATAGGGTT-3'
L23	5'-TTAGGGATTGGGATTGGGATTGGGTT-3'
L27	5'-TTAGGGTAAGGGAAAGGGTTTGGGTT-3'
L30	5'-TTAGGGTATGGGTTTGGGATAGGGTT-3'
L33	5'-TTAGGGTTAGGGTAAGGGATTGGGTT-3'
L37	5'-TTAGGGATAGGGATTGGGTTAGGGTT-3'
L41	5'-TTAGGGAAGGGTATGGGAAAGGGTT-3'

that all these sequences folded into G4 structures featured by different topologies (parallel, antiparallel and/or hybrid).^[55,56] Some of these oligonucleotides showed ability to form higher-order G4 species in addition to the monomeric ones, as evaluated by size exclusion high-performance liquid chromatography (SE-HPLC) analysis including,

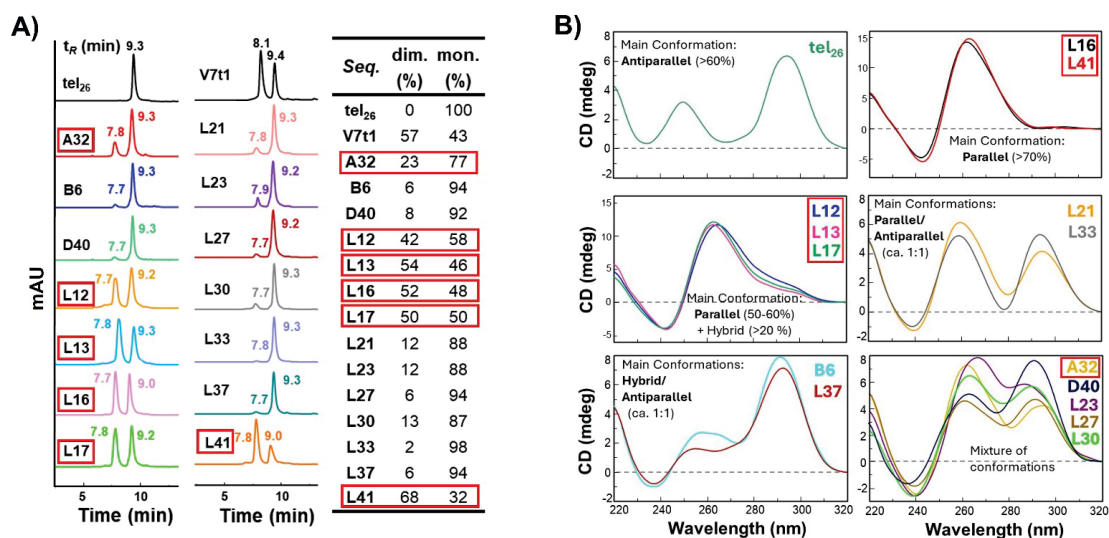


Figure 3. A) SE-HPLC analysis of the investigated oligonucleotides in PBS. The retention times (t_R) of monomeric and dimeric structures are indicated in correspondence to their relative peaks. In the Table, the percentage of monomeric (mon.) and dimeric (dim.) species formed by each analyzed sequence, as derived by integration of the chromatographic peaks, are reported. The red boxes highlighted the sequences with the highest percentage of dimeric species (> 20 %). B) Representative CD spectra of the indicated oligonucleotides in PBS grouped by conformational similarity. The figures are from Napolitano et al.,^[53] with permission.

as control oligonucleotides, tel₂₆, chosen as a reference for monomeric G4 structures, and the anti-VEGF aptamer V7t1 [57–59] able to fold into both monomeric and dimeric G4 species (Figure 3A). Interestingly, the combined use of circular dichroism (CD) and SE-HPLC analysis revealed that the sequences mainly adopting a parallel G4 topology (i.e., those named L12, L13, L16, L17 and L41), characterized by an intense CD band at around 260 nm (Figure 3B), were the ones with the highest percentage of dimeric species (sequences highlighted by red boxes in Figure 3A, including also A32 which formed 23 % of dimeric species).^[57,59] Notably, these dimeric parallel G4 structures exhibited high thermal stability, with melting temperatures near or higher than 60 °C, contrarily to the monomeric hybrid or antiparallel G4s (with CD bands of the main species between 290 and 295 nm) featured by lower thermal stability and T_m values close to 40 °C.

Chemiluminescence-based affinity assays showed that HMGB1 preferentially bound the aptamers forming the highest percentage of dimeric parallel G4 structures (Figure 4, red bars), whereas weaker affinities were found for the aptamers characterized by mainly monomeric hybrid or antiparallel G4s (Figure 4, orange and yellow bars).

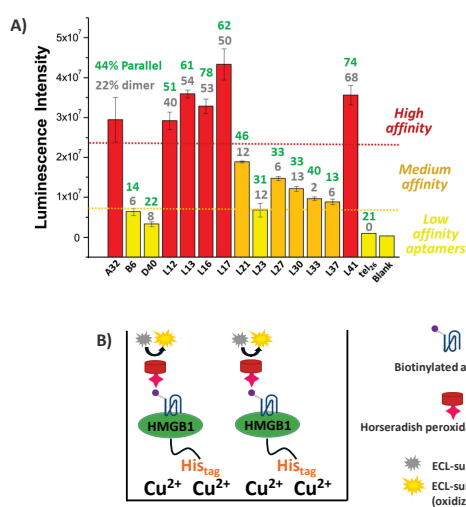


Figure 4. HMGB1-binding experiments. A) Chemiluminescence ELONA (Enzyme-Linked OligoNucleotide Assay) assays. On top of each column the percentages of dimeric species (down, in grey, determined on the basis of SE-HPLC analysis, Figure 3A) and of parallel conformation (up, in green) present in each oligonucleotide solution in PBS at 20 °C were indicated. Chemiluminescence intensity of the ECL (Enhanced ChemiLuminescence) substrate in the oxidized form was measured with a luminescence reader. Error bars indicate standard error (SD) values. B) Schematic representation of the ELONA assay.

Among all the identified aptamers, L12 emerged as the most promising candidate considering its overall features. In fact, it displayed strong binding affinity for HMGB1 (Figure 4), high thermal stability of its dimeric parallel G4 species (T_m = 61 °C) and an excellent serum resistance ($t_{1/2}$ > 48 h, Figure 5), as well as the best capacity to inhibit HMGB1-induced cell migration in NIH3T3 murine fibroblasts (IC_{50} = 28 nM, Figure 5) and in human A549 cancer cells (Figure 5).^[53] In addition, using the same chemiluminescence-based affinity assay described in Figure 4, it was proven that all the HMGB1 high-affinity aptamers (A32, L12, L13, L16, L17 and L41) displayed high selectivity for HMGB1 compared to other proteins, for which no binding was revealed, such as the circulating protein Galectin-3, and the membrane proteins Siglec-7 and CD19 (Figure 6). The same aptamers displayed medium affinity for VEGF-A,

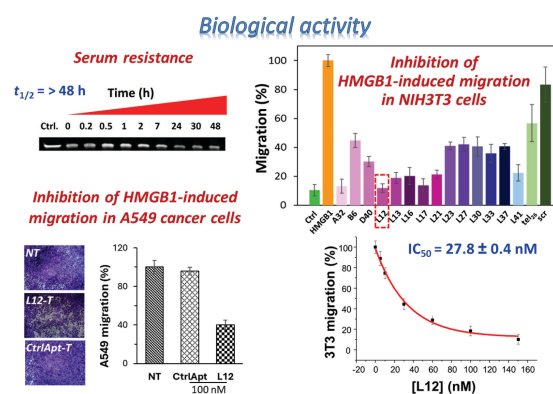


Figure 5. Anti-HMGB1 L12 aptamer biological activity. Serum resistance was measured by incubating the aptamer (10 μ M conc.) in 80 % FBS at 37 °C for 48 h and withdrawing at the indicated time points different aptamer aliquots, then loaded on a 20 % denaturing PAGE (Ctrl indicates the untreated oligonucleotide) the gel was run at constant 200 V at r.t. for 3 h in TBE, Tris/Borate/EDTA, 1x as running buffer, stained with GelGreen Nucleic Acid Stain and visualized with a UV transilluminator. Chemotaxis assays with NIH3T3 cells were performed by allowing cells to migrate in the presence of: i) serum-free medium (Ctrl, basal level of cell migration), ii) serum-free medium treated with 10 nM HMGB1 or iii) treated with 10 nM HMGB1 and 100 nM of each indicated aptamer or increasing concentrations of L12 (for the IC_{50} calculation). In the chemotaxis assays on human A549 lung cancer cells, cells were not-treated (NT) or treated for 24 h with 100 nM L12 (L12-T) or CtrlApt (non-G4-forming aptamer, negative control), and then allowed migrating for 24 h in the presence of 10 % FBS (representative images from migration assays). Cell migration is expressed as % with respect to the positive control (10 nM HMGB1 or NT cells). Error bars indicate SD values.

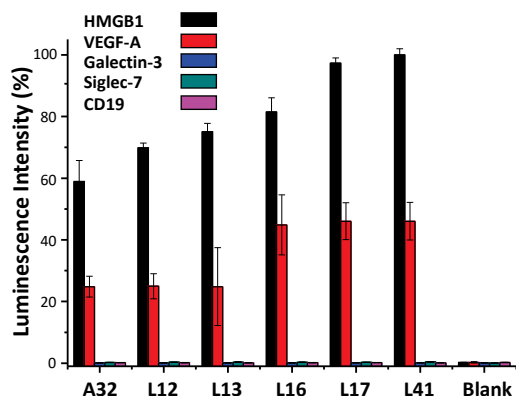


Figure 6. Evaluation of the affinity of the best-performing aptamers towards HMGB1, VEGF-A, Galectin-3, Siglec-7, CD19 proteins by ELONA assay. The luminescence intensity was normalized by setting the highest measured signal as 100 %. Error bars indicate SD values. The figure is from Napolitano et al.,^[53] with permission.

which, in analogy to HMGB1, is involved in cancer and inflammation and is known to be a G4-binding protein with high affinity for parallel G4-forming aptamers.^[57–59] However, among the indicated aptamers, L12 showed ability to bind this protein with ca. 3 times lower affinity than HMGB1 (Figure 6).

A more detailed analysis of the monomeric and dimeric species of L12, obtained as isolated species after

SE-HPLC separation, confirmed that the dimers were fully folded into parallel G4 structures, whereas the monomeric species mainly formed hybrid G4 structures (Figure 7). Interestingly, the isolated dimeric species of L12 proved to have much higher affinity than the monomeric one for the target protein (K_D values of ca. 26 vs. 104 nM, Figure 7). More notably, the dimeric L12 showed a significantly higher ability than its monomeric species to inhibit HMGB1-induced cell migration, with a behaviour similar to L12 analyzed as a mixture of both monomeric and dimeric forms, proving that the inhibition of cell migration of unseparated L12 was essentially due to its dimeric species. Altogether these data demonstrated that the best performance of L12 in PBS could be attributed to the presence, in solution, of its stable dimeric parallel G4 structures. As a general trend, many among the studied aptamer sequences were mainly structured into parallel G4 foldings forming significant amounts of dimeric species and these proved to be the most bioactive ones (cfr. Figures 3, 4 and 5).

Impact of Thermally Induced Unfolding/Refolding Processes on the Anti-HMGB1 Aptamers

In a subsequent study, we investigated how a standard thermal treatment of the anti-HMGB1 aptamers - specifically, an annealing procedure commonly used to reduce the polymorphism of oligonucleotide samples and favour the formation of thermodynamically stable conformations -

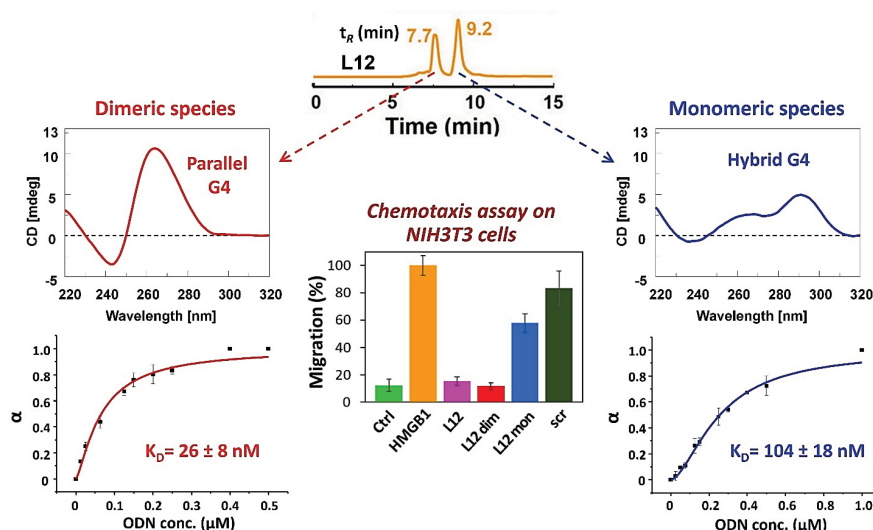


Figure 7. Main features of the separated dimeric and monomeric species of L12 aptamer. SE-HPLC profile of L12 in PBS (top); CD spectra (2 μ M oligonucleotide conc., 1 cm path length cell) and HMGB1-binding affinity assays (ELONA) of separated dimeric (left) and monomeric (right) L12 species. In the middle, chemotaxis assay on NIH3T3 cells (4 h incubation at 37 °C): serum-free medium (Ctrl, negative control), serum-free medium with either only 10 nM HMGB1 (positive control) or 10 nM HMGB1 added with 100 nM of each indicated sample. Cell migration is expressed as % with respect to the positive control (error bars indicate SD values).

affected the structure and bioactivity of the previously selected HMGB1-targeting aptamers.^[60] Strikingly, SE-HPLC analysis revealed that, in a pseudo-physiological solution, an annealing process - consisting in heating the samples at high temperature (generally 95 °C) for 5 min and then very slowly cooling them to r.t. - led to irreversible loss of the dimeric species in favour of the monomeric ones (cfr. Figure 8A with Figure 3A). TDS (thermal difference spectra) were obtained for all the investigated sequences, which together with CD spectra analysis (Figure 8B) proved that all the aptamers, even after a heating/cooling cycle, formed G4 structures. However, in the case of L16 and L41 the TDS were not easily interpretable probably because of the concurrent presence of G4 structures and random coil forms.

Furthermore, many of the studied aptamers evidenced a marked conformational change upon annealing, switching from parallel to predominantly hybrid or antiparallel G4 foldings, as assessed on the basis of their CD spectra (cfr. Figure 8B with Figure 3B).

In almost all cases after annealing (A.) the aptamers formed monomeric G4 structures with a reduced thermal stability (T_m values often lower than or close to 37 °C in PBS), especially those containing high percentages of dimeric species when in not-annealed (N.A.) form (Table 2). Only three sequences, i.e. D40, L30 and L33, showed apparent T_m values of their main G4 conformations higher than 44 °C. All the annealed aptamers exhibited also a reduced enzymatic resistance in serum ($t_{1/2} \cong 1\text{--}4$ h vs. ca. 48 h for the not-annealed aptamers mainly characterized by parallel dimeric G4 species) and a significantly decreased affinity for HMGB1, compared to the same samples not subjected to annealing.

Table 2. CD-derived apparent melting temperature (T_m) values for the selected aptamers and tel₂₆ control sequence. A comparison between not-annealed (N.A.) and annealed (A.) samples was performed.

Seq.	$T_m \pm 1$ / °C	$T_m \pm 1$ / °C
	A. (main conformations)	N.A. (main conformations)
tel ₂₆	51 (295)	53 (295)
A32	39 (295)	63 (262)
B6	43 (292)	44 (291)
D40	48 (291)	48 (291)
L12	36 (291)	61 (265)
L13	30 (292)	61 (262)
L16	n.d.	57 (262)
L17	35 (292)	62 (264)
L21	44 (295)	42 (295)
L23	36 (291)	32 (296)
L27	40 (293)	36 (292)
L30	45 (292)	42 (290)
L33	47 (293)	49 (295)
L37	42 (292)	43 (292)
L41	n.d.	61 (263)

In particular, a chemiluminescent HMGB1-binding assay evidenced for L30 - selected as the oligonucleotide with the best thermal and enzymatic stabilities in the series of the annealed aptamers ($T_m = 45$ °C and $t_{1/2} = 3.6$ h) - a K_D value of 214 ± 26 nM. This was indicative of an affinity for the target protein ca. 10-fold lower than the best not-

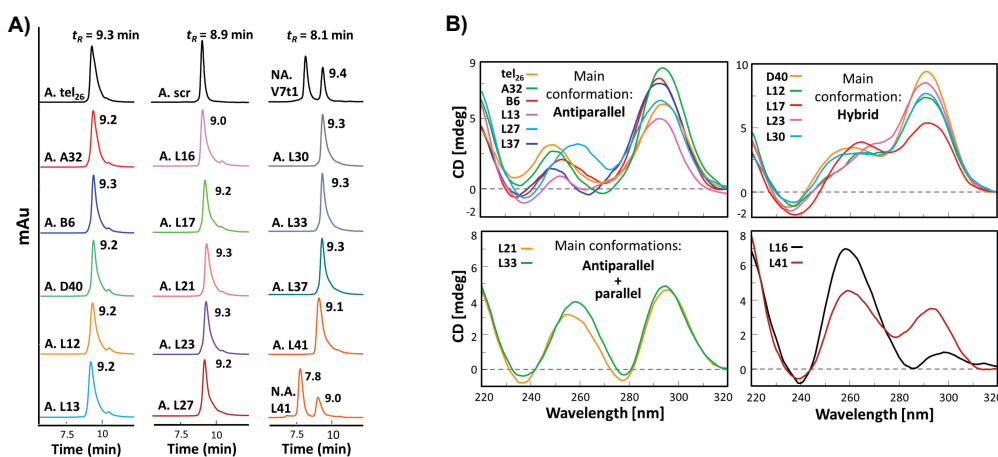


Figure 8. A) Representative SE-HPLC analysis chromatograms of the investigated oligonucleotides after annealing (indicated as A.) in PBS; N.A. (i.e. not-annealed) V7t1 and L41 were used as controls for the dimeric species; the retention times (t_R) of dimeric and monomeric structures are indicated in correspondence to the relative peaks. B) Representative CD spectra (2 μ M oligonucleotide conc., 1 cm path length cell) of the indicated oligonucleotides, after annealing in PBS, grouped based on conformational similarity. The figure is adapted from Napolitano et al.,^[60] with permission.

annealed aptamer previously investigated, i.e. the isolated dimeric species of L12, featured by a K_D value of ca. 26 nM. More importantly, the ability to inhibit HMGB1-induced cell migration of these representative aptamers, i.e. L30 (for the series of the annealed aptamers) and L12 (for the not-annealed aptamers), analyzed in both their annealed and not-annealed forms, was evaluated by chemotaxis assays on BALB/c 3T3 cells at 37 °C. In detail, in the annealed form L12 (mainly structured into a monomeric hybrid G4 structure) proved to be ca. 3-fold less active than its not-annealed counterpart, whereas L30 showed a similar activity, no matter whether annealed or not (Figure 9). These data fully confirmed our overall picture, showing that a higher anti-HMGB1 activity can be mainly attributable to the presence of dimeric parallel G4 structures, which have higher affinity than the monomeric G4 structures for the target protein. Thus, we had clear experimental evidence that the higher is the dimer percentage in each not-annealed aptamer (cfr. 40 % for L12 and 13 % for L30), the higher is the difference in the aptamer inhibitory activity observed on comparing its annealed with the not-annealed form (Figure 9). Interestingly, L30 and L12, when in the annealed form, showed very similar inhibitory activity towards HMGB1-induced cell migration (light blue vs. lilac bar, Figure 9), plausibly because, in addition to being both monomeric, they showed also similar G4 topology, being mainly hybrid G4 structures (Figure 9). However, it is to be

noted that in both cases the tested annealed aptamers proved to exert significant inhibitory effects on HMGB1-induced cell migration when compared to the negative controls tel₂₆ and scr (Figure 9).

Thus, in summary, the set of G-quadruplex-forming aptamers we selected as HMGB1 inhibitors generally showed different properties strictly depending on their manipulation, and particularly if subjected to standard annealing procedure or not. This procedure is a critical step potentially leading to irreversible loss of spontaneously formed conformations, which could be kinetically but not thermodynamically preferred (as in the case of the dimeric parallel G4 structures of L12 and other aptamers), and its effects should thus be always carefully controlled.

Locking the Aptamers in Their Dimeric G4 Bioactive Species

The above reported data demonstrated that L12 was the best inhibitor of HMGB1 in a pseudo-physiological buffer but only if its working solutions were obtained upon dilution of a highly concentrated stock at r.t., without subjecting the samples to thermal treatments at temperatures above its melting temperature ($T_m = 61$ °C). As explained above, this thermal treatment irreversibly destroyed its dimeric parallel G4 structures, formed by spontaneous self-assembly, which showed much higher affinity and inhibitory activity towards the target protein than its monomeric form.

In this frame, a focused set of covalently linked L12 dimers was then realized to lock this oligonucleotide in its bioactive dimeric G4 conformation.^[61] In this new design, two L12 oligonucleotide sequences were connected using linkers of different nature and length, allowing them to maintain or invert their relative polarity (Figure 10). In detail, thymidine-based linkers (indicated as T) containing 1, 2, 4 or 7 nucleotide units, a triethylene glycol-based linker (indicated as Spacer 9 or S9, with approximately the length of a dinucleotide), and a symmetric doubler (indicated as D, spanning approximately the length of a trinucleotide) were exploited (Figure 10).

Biophysical characterization showed that all the covalent dimers with 3'-3' or 5'-5' inversion of polarity sites formed parallel G4 conformations, mimicking the bioactive L12 dimeric species, whereas those with continuous 5'-3' polarity along the strand adopted mainly hybrid G4 structures (Figure 11).

Interestingly, the highest affinity for the target protein was found for L12d1T3 and L12d1T5, with K_D values of 44 ± 5 and 56 ± 5 nM, respectively, demonstrating that the affinity for HMGB1 did not exclusively depend on the G4 conformation but also on the nature and length of the linker used for the aptamer dimerization. Indeed, these covalent dimers were characterized not only by a 3'-3' and

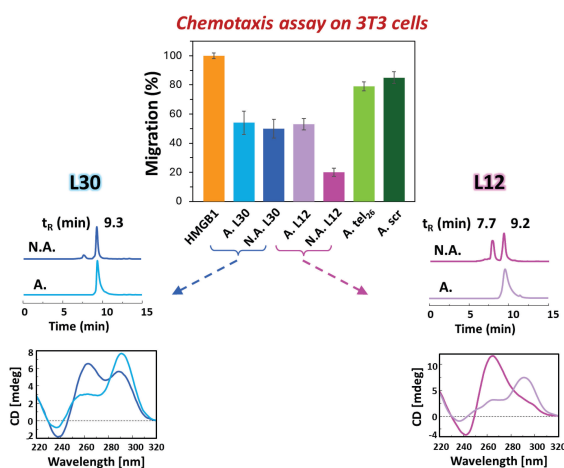


Figure 9. Chemotaxis assays on BALB/c 3T3 cells (top; 4 h incubation at 37 °C): serum-free medium with 10 nM HMGB1 (positive control) and 10 nM HMGB1 combined with 100 nM of each indicated oligonucleotide; cell migration is expressed as % with respect to the positive control (error bars indicate SD values). SE-HPLC profiles and overlapped CD spectra (1 cm path length cell) of L30 (left) and L12 (right) in their not-annealed and annealed form in PBS (2 μ M oligonucleotide conc.).

Linkers investigated

Thymidine 5'-monophosphate = T

Doubler = D

Spacer 9 = S9

Dimer name	Linker type	Strands connection	Sequence	Length
L12d1T	1T	3'-5'	5'TAGGGATTGGGAATGGGTATGGGT ^{3'} T ^{5'} TAGGGATTGGGAATGGGTATGGGT ^{3'}	53-mer
L12d2T	2T	3'-5'	5'TAGGGATTGGGAATGGGTATGGGT ^{3'} TT ^{5'} TAGGGATTGGGAATGGGTATGGGT ^{3'}	54-mer
L12d4T	4T	3'-5'	5'TAGGGATTGGGAATGGGTATGGGT ^{3'} TTTT ^{5'} TAGGGATTGGGAATGGGTATGGGT ^{3'}	56-mer
L12d7T	7T	3'-5'	5'TAGGGATTGGGAATGGGTATGGGT ^{3'} TTTTTT ^{5'} TAGGGATTGGGAATGGGTATGGGT ^{3'}	59-mer
L12d1T3	1T	3'-3'	5'TAGGGATTGGGAATGGGTATGGGT ^{3'} T ^{5'} TGGGTATGGTAAGGGTTAGGGATT ^{5'}	53-mer
L12d1T5	1T	5'-5'	3'TGGGTATGGTAAGGGTTAGGGATT ^{5'} T ^{5'} TAGGGATTGGGAATGGGTATGGGT ^{3'}	53-mer
L12dS9	S9	3'-5'	5'TAGGGATTGGGAATGGGTATGGGT ^{3'} S9 ^{5'} TAGGGATTGGGAATGGGTATGGGT ^{3'}	52-mer + S9
L12dS95	S9	5'-5'	3'TGGGTATGGTAAGGGTTAGGGATT ^{5'} S9 ^{5'} TAGGGATTGGGAATGGGTATGGGT ^{3'}	52-mer + S9
L12dD3	D	3'-3'	5'TAGGGATTGGGAATGGGTATGGGT ^{3'} D ^{5'} TGGGTATGGTAAGGGTTAGGGATT ^{5'}	52-mer + D
L12dFB	No linker	3'-5'	5'TAGGGATTGGGAATGGGTATGGGTAGGGATTGGGAATGGGTATGGGT ^{3'}	50-mer

Figure 10. Upper panel: hemical structures of the linkers used to obtain the here studied covalently linked L12 dimers; lower panel: list of the covalently linked L12 dimers, their sequences and main features.

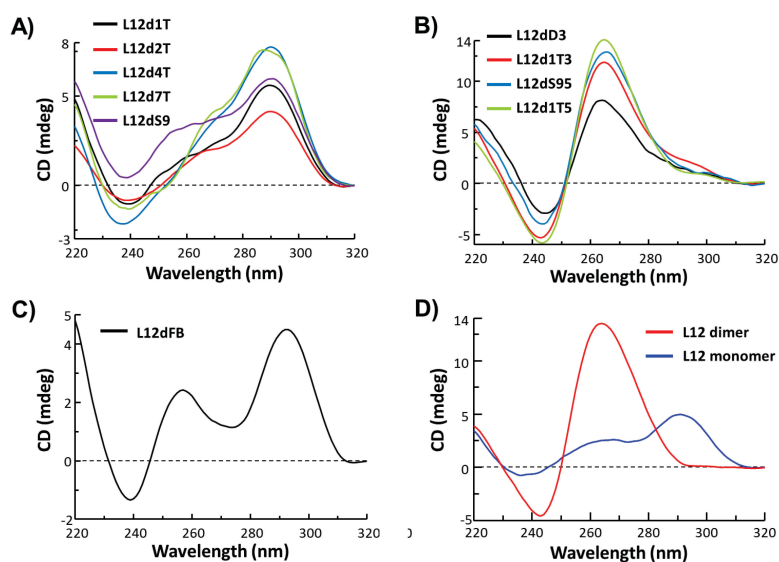


Figure 11. Representative CD spectra of the covalently linked L12 dimers grouped by G4 conformational similarity (panels A-C), and of the non-covalent dimeric and monomeric L12 species (panel D). The figure is adapted from Criscuolo et al.^[61]

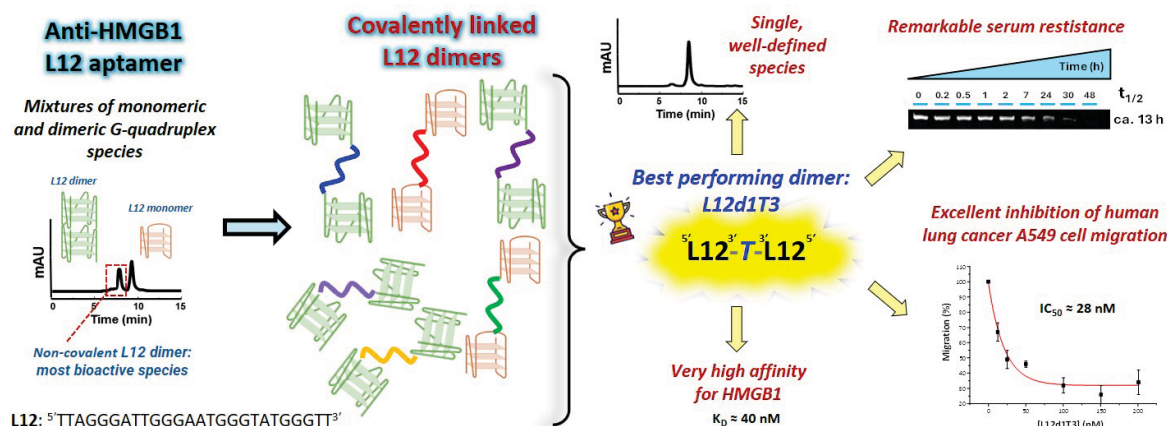


Figure 12. Schematic representation of the general design of the covalently linked L12 dimers and main properties of the best candidate, named L12d1T3.^[61]

5'-5' inversion of polarity site, guaranteeing parallel G4 conformations, but also by a short, more rigid linker (a single T unit), instead of longer or more flexible ones (as D and S95). The overall results designated L12d1T3 as the best dimeric aptamer of the series, showing also the highest resistance to nuclease degradation ($t_{1/2} = 13$ h) and marked ability to inhibit HMGB1-induced cell migration (IC_{50} value of *ca.* 28 nM) on A549 lung cancer cells (Figure 12). Moreover, this aptamer proved to be superior to the spontaneously formed L12 non-covalent dimer, representing a valuable ready-to-use, unimolecular variant of the most bioactive species featured by essentially reversible folding/unfolding processes.^[61]

CONCLUSIONS AND FUTURE PERSPECTIVES

The combined results of the here described studies outline a clear roadmap to obtain effective HMGB1-targeting aptamers. In detail, the overall studies we have carried out in this field led to a rich set of data which, even in the absence of detailed structural information, can provide a consistent structure-activity relationship picture. First of all, we demonstrated that the spontaneous dimerization in parallel G4 structures is a crucial event for obtaining anti-HMGB1 aptameric systems endowed with high thermal and enzymatic stability, along with high affinity and bioactivity. Then, the conventional annealing procedure, commonly used to reduce the polymorphism of the investigated oligonucleotides, can be in our case detrimental, destroying the spontaneously formed dimeric/oligomeric species of our best aptamers, as is the case of L12, having the best bioactivity. Finally, covalently linking two monomeric L12

sequences with a proper linker proved to be a valuable strategy^[62] to lock the bioactive dimeric conformations and enhance the properties of this aptamer. The best results were obtained with a thymidine linker and 3'-3' inversion of polarity site, allowing us to speculate that its 3D conformation could be quite similar to the overall arrangement of the non-covalent dimeric species that is spontaneously formed by L12. Notably, this design led to a single, well-defined covalently linked L12-dimer with a reversible folding/unfolding profile and thus in principle ideal candidate for therapeutic and theranostic applications in HMGB1-related pathologies, especially inflammation and cancer.

Further optimization of the selected aptamers is currently ongoing in our laboratories. On the aptamers proved to be the best protein binders, modifications will be introduced aiming at further improving their thermal stability and nuclease resistance, crucial parameters for their effective use as potential drugs. As a general optimization strategy, single modifications can be considered at different positions of their skeleton. Locked nucleic acids (LNAs), i.e. 2'-O-4'-C-methylene-linked bicyclic ribonucleoside monomers, will be introduced as useful conformationally constrained surrogates of natural nucleotides. The influence of LNA modifications on G-quadruplex structures has been extensively studied.^[63–65] Indeed, the insertion of LNA monomers in specific positions of an aptamer can improve not only its stability, but also its bioactivity on cancer cells^[66]. Another strategy for aptamer optimization will involve the use of 2'-deoxy-2'-fluoro-D-arabinonucleic acid (2'-F-ANA) modifications.^[67] Indeed, modifications with 2'-F-ANA nucleotides is an approach already successfully investigated in other G-quadruplex-forming aptamers, providing enhanced stability and nuclease resistance in the final systems.^[67,68]

Structural analysis of these systems is also under investigation in collaboration with specialized research groups expert in NMR spectroscopy, mass spectrometry and crystallography. These studies are of crucial importance and will provide precious structural insights into these G4-forming aptamers, allowing, on one hand, the identification of their conformational preferences in pseudo-physiological solutions and, on the other, the rational design of modified analogues as even more effective and selective anti-HMGB1 aptamers for in vivo investigations.

Acknowledgment. The research leading to these results has received funding from: i) Fondazione AIRC under IG 2020—ID.25046 — P.I. Montesarchio Daniela; 2) CN00000041 National Center for Gene Therapy and Drugs based on RNA Technology and the European Union-NextGeneration EU — P.I. Montesarchio Daniela; iii) Federico II University, FRA2022 project (CUP: E65F22000050001) — P.I. Musumeci Domenica.

REFERENCES

- [1] G. H. Goodwin, C. Sanders, E. W. Johns, *Eur J Biochem* **1973**, *38*, 14–19.
<https://doi.org/10.1111/j.1432-1033.1973.tb03026.x>
- [2] D. Tang, R. Kang, H. J. Zeh, M. T. Lotze, *Nat Rev Immunol* **2023**, *23*, 824–841.
<https://doi.org/10.1038/s41577-023-00894-6>
- [3] C. M. Read, P. D. Cary, C. Crane-Robinson, P. C. Driscoll, D. G. Norman, *Nucleic Acids Res* **1993**, *21*, 3427–3436.
<https://doi.org/10.1093/nar/21.15.3427>
- [4] H. M. Weir, P. J. Kraulis, C. S. Hill, A. R. C. Raine, E. D. Laue, J. O. Thomas, *EMBO J* **1993**, *12*, 1311–1319.
<https://doi.org/10.1002/j.1460-2075.1993.tb05776.x>
- [5] C. H. Hardman, R. William Broadhurst, A. R. C. Raine, K. D. Grasser, J. O. Thomas, E. D. Laue, *Biochemistry* **1995**, *34*, 16596–16607.
<https://doi.org/10.1021/bi00051a007>
- [6] Q. Wang, M. Zeng, W. Wang, J. Tang, *Biochem Biophys Res Commun* **2007**, *360*, 14–19.
<https://doi.org/10.1016/j.bbrc.2007.05.130>
- [7] T. Bonaldi, G. Längst, R. Strohnner, P. B. Becker, M. E. Bianchi, *EMBO Journal* **2002**, *21*, 6865–6873.
<https://doi.org/10.1093/emboj/cdf692>
- [8] I. Ugrinova, I. G. Pashev, E. A. Pasheva, *Biochemistry* **2009**, *48*, 6502–6507.
<https://doi.org/10.1021/bi9004304>
- [9] D. Topalova, I. Ugrinova, I. G. Pashev, E. A. Pasheva, *Int J Biochem Cell Biol* **2008**, *40*, 1536–1542.
<https://doi.org/10.1016/j.biocel.2007.11.014>
- [10] K. Fujita, K. Motoki, K. Tagawa, X. Chen, H. Hama, K. Nakajima, H. Homma, T. Tamura, H. Watanabe, M. Katsuno, C. Matsumi, M. Kajikawa, T. Saito, T. Saido, G. Sobue, A. Miyawaki, H. Okazawa, *Sci Rep* **2016**, *6*, 31895. <https://doi.org/10.1038/srep31895>
- [11] F. Z. Ikram, A. Arulsamy, T. Retinasamy, Mohd. F. Shaikh, *Curr Neuropharmacol* **2022**, *20*, 2221–2245.
<https://doi.org/10.2174/1570159X20666220114153308>
- [12] Y. N. Paudel, E. Angelopoulou, C. Piperi, I. Othman, K. Aamir, M. F. Shaikh, *Cells* **2020**, *9*, 383.
<https://doi.org/10.3390/cells9020383>
- [13] P. Scaffidi, T. Misteli, M. E. Bianchi, *Nature* **2002**, *418*, 191–195.
<https://doi.org/10.1038/nature00858>
- [14] G. Li, X. Liang, M. T. Lotze, *Front Immunol* **2013**, *4*, 1–9. <https://doi.org/10.3389/fimmu.2013.00068>
- [15] R. Kang, R. Chen, Q. Zhang, W. Hou, S. Wu, L. Cao, J. Huang, Y. Yu, X. G. Fan, Z. Yan, X. Sun, H. Wang, Q. Wang, A. Tsung, T. R. Billiar, H. J. Zeh, M. T. Lotze, D. Tang, *Mol Aspects Med* **2014**, *40*, 1–116.
<https://doi.org/10.1016/j.mam.2014.05.001>
- [16] R. Palumbo, F. De Marchis, T. Pusterla, A. Conti, M. Alessio, M. E. Bianchi, *J Leukoc Biol* **2009**, *86*, 617–623. <https://doi.org/10.1189/jlb.0908581>
- [17] R. Kokkola, Å. Andersson, G. Mullins, T. Östberg, C. J. Treutiger, B. Arnold, P. Nawroth, U. Andersson, R. A. Harris, H. E. Harris, *Scand J Immunol* **2005**, *61*, 1–9.
<https://doi.org/10.1111/j.0300-9475.2005.01534.x>
- [18] J. Todorova, E. Pasheva, *Oncol Lett* **2012**, *3*, 214–218.
<https://doi.org/10.3892/ol.2011.459>
- [19] M. Kerkeni, J. Gharbi, *Med Hypotheses* **2020**, *144*, 1–2. <https://doi.org/10.1016/j.mehy.2020.109950>
- [20] W. Ren, L. Zhao, Y. Sun, X. Wang, X. Shi, *Molecular Medicine* **2023**, *29*, 117.
<https://doi.org/10.1186/s10020-023-00717-3>
- [21] E. Ranzato, S. Martinotti, M. Patrone, *Immunotargets Ther* **2015**, *4*, 101–109.
<https://doi.org/10.2147/ITT.S58064>
- [22] B. DeWulf, L. Minsart, F. Verdonk, V. Kruys, M. Piagnerelli, M. Maze, S. Saxena, *Cells* **2023**, *12*, 1088.
<https://doi.org/10.3390/cells12071088>
- [23] U. Andersson, H. Wang, K. Palmblad, A. C. Aveberger, O. Bloom, H. Erlandsson-Harris, A. Janson, R. Kokkola, M. Zhang, H. Yang, K. J. Tracey, *Journal of Experimental Medicine* **2000**, *192*, 565–570. <https://doi.org/10.1084/jem.192.4.565>
- [24] I. Kaur, T. Behl, S. Bungau, A. Kumar, V. Mehta, D. Setia, M. S. Uddin, G. Zengin, L. Aleya, S. Arora, *Life Sci* **2020**, *258*, 118164.
<https://doi.org/10.1016/j.lfs.2020.118164>
- [25] F. Li Pomi, F. Borgia, P. Custurone, M. Vaccaro, G. Pioggia, S. Gangemi, *Int J Mol Sci* **2022**, *23*, 1–18.
<https://doi.org/10.3390/ijms23169327>

- [26] D. Süren, M. Yildirim, Ö. Demirpençe, V. Kaya, A. S. Alikanoğlu, N. Bülbüller, M. Yildiz, C. Sezer, *Medical Science Monitor* **2014**, *20*, 530–537.
<https://doi.org/10.12659/MSM.890531>
- [27] L. Zhu, S. Ren, M. J. Daniels, W. Qiu, L. Song, T. You, D. Wang, Z. Wang, *Front Med (Lausanne)* **2021**, *8*, 1–10. <https://doi.org/10.3389/fmed.2021.756988>
- [28] N. A. Handke, A. B. A. Rupp, N. Trimpop, J. von Pawel, S. Holdenrieder, *Diagnostics* **2021**, *11*, 356.
<https://doi.org/10.3390/diagnostics11020356>
- [29] A. Di Lorenzo, E. Bolli, R. Ruiiu, G. Ferrauto, E. Di Gregorio, L. Avalue, A. Savino, P. Poggio, I. F. Merighi, F. Riccardo, M. Brancaccio, E. Quaglino, F. Cavallo, L. Conti, *Oncoimmunology* **2022**, *11*, 1–18.
<https://doi.org/10.1080/2162402X.2022.2086752>
- [30] L. Lupu, A. Palmer, M. Huber-lang, *Front Immunol* **2020**, *11*, 1–11.
<https://doi.org/10.3389/fimmu.2020.584514>
- [31] D. Musumeci, G. N. Roviello, D. Montesarchio, *Pharmacol Ther* **2014**, *141*, 347–357.
<https://doi.org/10.1016/j.pharmthera.2013.11.001>
- [32] J. Xue, J. S. Suarez, M. Minaai, S. Li, G. Gaudino, H. I. Pass, M. Carbone, H. Yang, *J Cell Physiol* **2021**, *236*, 3406–3419. <https://doi.org/10.1002/jcp.30125>
- [33] Y. Yamamura, T. Santa, H. Kotaki, K. Uchino, Y. Sawada, T. Iga, *Biol Pharm Bull* **1995**, *18*, 337–341.
<https://doi.org/10.1248/bpb.18.337>
- [34] J. Li, X. Fan, Q. Wang, *Medicine (United States)* **2018**, *97*, e0073.
<https://doi.org/10.1097/MD.00000000000010073>
- [35] S. Bindu, S. Mazumder, U. Bandyopadhyay, *Biochem Pharmacol* **2020**, *180*, 114147.
<https://doi.org/10.1016/j.bcp.2020.114147>
- [36] J. Sgrignani, V. Cecchinato, E. M. A. Fassi, G. D'Agostino, M. Garofalo, G. Danelon, M. Pedotti, L. Simonelli, L. Varani, G. Grazioso, M. Ugucioni, A. Cavalli, *J Med Chem* **2021**, *64*, 13439–13450.
<https://doi.org/10.1021/acs.jmedchem.1c00852>
- [37] T. Adachi, Y. Nakamura, *Molecules* **2019**, *24*, 4229.
<https://doi.org/10.3390/molecules24234229>
- [38] S. Burge, G. N. Parkinson, P. Hazel, A. K. Todd, S. Neidle, *Nucleic Acids Res* **2006**, *34*, 5402–5415.
<https://doi.org/10.1093/nar/gkl655>
- [39] Y. Ma, K. Iida, K. Nagasawa, *Biochem Biophys Res Commun* **2020**, *531*, 3–17.
<https://doi.org/10.1016/j.bbrc.2019.12.103>
- [40] L. Li, S. Xu, H. Yan, X. Li, H. S. Yazd, X. Li, T. Huang, C. Cui, J. Jiang, W. Tan, *Angew Chem Int Ed.* **2021**, *60*, 2221–2231.
<https://doi.org/10.1002/anie.202003563>
- [41] M. Egli, M. Manoharan, *Nucleic Acids Res* **2023**, *51*, 2529–2573.
<https://doi.org/10.1093/nar/gkad067>
- [42] A. Brown, J. Brill, R. Amini, C. Nurmi, Y. Li, *Angew Chem Int Ed.* **2024**, *63*, e2023118665.
<https://doi.org/10.1002/anie.202318665>
- [43] C. Platella, C. Riccardi, D. Montesarchio, G. N. Roviello, D. Musumeci, *Biochim Biophys Acta* **2017**, *1861*, 1429–1447.
<https://doi.org/10.1016/j.bbagen.2016.11.027>
- [44] M. E. Bianchi, M. Beltrame, G. Paonessa, *Science* (1979) **1989**, *243*, 1056–1059.
<https://doi.org/10.1126/science.2922595>
- [45] E. M. Bucci, M. Valente, D. Musumeci, R. Sapio, V. Anrò, G. N. Roviello, M. Moccia, *Nucleosides Nucleotides Nucleic Acids* **2007**, *26*, 1047–1050.
<https://doi.org/10.1080/15257770701509602>
- [46] D. Musumeci, E. M. Bucci, G. N. Roviello, R. Sapio, M. Valente, M. Moccia, M. E. Bianchi, C. Pedone, *Mol Biosyst* **2011**, *7*, 1742–1752.
<https://doi.org/10.1039/c1mb05009e>
- [47] D. Rentzeperis, J. Ho, L. A. Marky, *Biochemistry* **1993**, *32*, 2564–2572.
<https://doi.org/10.1021/bi00061a014>
- [48] S. Antsyppovich, E. Kubareva, V. Tashlitsky, T. Oretskaya, Z. Shabarova, *Eur J Biochem* **1998**, *255*, 414–421.
<https://doi.org/10.1046/j.1432-1327.1998.2550414.x>
- [49] D. Musumeci, G. N. Roviello, D. Montesarchio, R. Sapio, M. Valente, V. Anrò, E. M. Bucci, *RSC Adv* **2013**, *3*, 12176–12184.
<https://doi.org/10.1039/c3ra41915k>
- [50] B. Pagano, L. Margarucci, P. Zizza, J. Amato, N. Iaccarino, C. Cassiano, E. Salvati, E. Novellino, A. Biroccio, A. Casapullo, A. Randazzo, *Chem Comm* **2015**, *51*, 2964–2967.
<https://doi.org/10.1039/C4CC07231F>
- [51] J. Amato, L. Cerofolini, D. Brancaccio, S. Giuntini, N. Iaccarino, P. Zizza, S. Iachettini, A. Biroccio, E. Novellino, A. Rosato, M. Fragai, C. Luchinat, A. Randazzo, B. Pagano, *Nucleic Acids Res* **2019**, *47*, 9950–9966. <https://doi.org/10.1093/nar/gkz727>
- [52] J. Amato, T. W. Madanayake, N. Iaccarino, E. Novellino, A. Randazzo, L. H. Hurley, B. Pagano, *Chem Comm* **2018**, *54*, 9442–9445.
<https://doi.org/10.1039/C8CC03614D>
- [53] E. Napolitano, A. Criscuolo, C. Riccardi, C. L. Esposito, S. Catuogno, G. Coppola, G. N. Roviello, D. Montesarchio, D. Musumeci, *Angew Chem Int Ed* **2024**, *63*, e202319828. <https://doi.org/10.1002/anie.202319828>
- [54] C. Riccardi, E. Napolitano, C. Platella, D. Musumeci, D. Montesarchio, *Med. Res. Rev.* **2020**, *41*, 464–506.
<https://doi.org/10.1002/med.21737>
- [55] R. Del Villar-Guerra, R. D. Gray, J. B. Chaires, *Curr Protoc Nucleic Acid Chem* **2017**, *2017*, 17.8.1–17.8.16. <https://doi.org/10.1002/cpnc.23>

- [56] R. del Villar-Guerra, J. O. Trent, J. B. Chaires, *Angew Chem Int Ed* **2018**, 57, 7171–7175.
<https://doi.org/10.1002/anie.201709184>
- [57] F. Moccia, C. Riccardi, D. Musumeci, S. Leone, R. Oliva, L. Petraccone, D. Montesarchio, *Nucleic Acids Res* **2019**, 47, 8318–8331. <https://doi.org/10.1093/nar/gkz589>
- [58] C. Riccardi, D. Musumeci, C. Platella, R. Gaglione, A. Arciello, D. Montesarchio, *Int J Mol Sci* **2020**, 21, 1–24. <https://doi.org/10.3390/ijms21061963>
- [59] E. Napolitano, C. Riccardi, R. Gaglione, A. Arciello, V. Pirota, A. Triveri, F. Doria, D. Musumeci, D. Montesarchio, *Int J Biol Macromol* **2023**, 224, 344–357. <https://doi.org/10.1016/j.ijbiomac.2022.10.128>
- [60] E. Napolitano, A. Criscuolo, C. Riccardi, C. Platella, R. Gaglione, A. Arciello, D. Musumeci, D. Montesarchio, *Int J Biol Macromol* **2024**, 283, 137148. <https://doi.org/10.1016/j.ijbiomac.2024.137148>
- [61] A. Criscuolo, E. Napolitano, C. Riccardi, R. Gaglione, E. Piccolo, A. Arciello, D. Musumeci, D. Montesarchio, *Int J Biol Macromol*, **2025**, 332, 148479. doi: 10.1016/j.ijbiomac.2025.148479
- [62] C. Riccardi, E. Napolitano, D. Musumeci, D. Montesarchio, *Molecules* **2020**, 25, 7–15. <https://doi.org/10.3390/molecules25225227>
- [63] O. Doluca, J. M. Withers, V. V. Filichev, *Chem Rev* **2013**, 113, 3044–3083. <https://doi.org/10.1021/cr300225q>
- [64] C. Roxo, A. Pasternak, *PLoS One* **2022**, 17, e0273528. <https://doi.org/10.1371/journal.pone.0273528>
- [65] H. Doessing, B. Vester, *Molecules* **2011**, 16, 4511–4526. <https://doi.org/10.3390/molecules16064511>
- [66] S. L. Edwards, V. Poongavanam, J. R. Kanwar, K. Roy, K. M. Hillman, N. Prasad, R. Leth-Larsen, M. Petersen, M. Marušič, J. Plavec, J. Wengel, R. N. Veedu, *Chem Comm* **2015**, 51, 9499–9502. <https://doi.org/10.1039/C5CC02756J>
- [67] C. G. Peng, M. J. Damha, *Nucleic Acids Res* **2007**, 35, 4977–4988. <https://doi.org/10.1093/nar/gkm520>
- [68] R. El-Khoury, M. J. Damha, *Acc Chem Res* **2021**, 54, 2287–2297. <https://doi.org/10.1021/acs.accounts.1c00125>